Published in final edited form as:
Dev Cell. 2014 June 23; 29(6): 701–715. doi:10.1016/j.devcel.2014.05.011.

Dynamic Control of Excitatory Synapse Development by a Rac1 GEF/GAP Regulatory Complex

Kyongmi Um[1], **Sanyong Niu**[1], **Joseph G. Duman**[1], **Jinxuan Cheng**[1,2], **Yen-Kuei Tu**[1,3], **Brandon Schwechter**[1], **Feng Liu**[1], **Laura Hiles**[1], **Anjana Narayanan**[1,2], **Ryan T. Ash**[1], **Shalaka Mulherkar**[1], **Kannan Alpadi**[2], **Stelios M. Smirnakis**[1], and **Kimberley F. Tolias**[1,2,3,*]

[1]Department of Neuroscience, Baylor College of Medicine, One Baylor Plaza, Houston, TX 77030, USA

[2]Verna and Marrs McLean Department of Biochemistry and Molecular Biology, Baylor College of Medicine, One Baylor Plaza, Houston, TX 77030, USA

[3]Integrative Molecular and Biomedical Sciences Program, Baylor College of Medicine, One Baylor Plaza, Houston, TX 77030, USA

SUMMARY

The small GTPase Rac1 orchestrates actin-dependent remodeling essential for numerous cellular processes including synapse development. While precise spatiotemporal regulation of Rac1 is necessary for its function, little is known about the mechanisms that enable Rac1 activators (GEFs) and inhibitors (GAPs) to act in concert to regulate Rac1 signaling. Here we identify a regulatory complex composed of a Rac-GEF (Tiam1) and a Rac-GAP (Bcr) that cooperate to control excitatory synapse development. Disruption of Bcr function within this complex increases Rac1 activity and dendritic spine remodeling, resulting in excessive synaptic growth that is rescued by Tiam1 inhibition. Notably, EphB receptors utilize the Tiam1-Bcr complex to control synaptogenesis. Following EphB activation, Tiam1 induces Rac1-dependent spine formation, whereas Bcr prevents Rac1-mediated receptor internalization, promoting spine growth over retraction. The finding that a Rac-specific GEF/GAP complex is required to maintain optimal levels of Rac1 signaling provides an important insight into the regulation of small GTPases.

INTRODUCTION

Most excitatory synapses in the brain are located on dendritic spines, small actin-rich dendritic protrusions. Spines undergo rapid remodeling during development and in response to physiological stimuli. This remodeling, driven by actin dynamics, is critical for the formation and refinement of neuronal circuits and for synaptic plasticity associated with

*Corresponding author: Kimberley F. Tolias, Ph.D., Department of Neuroscience, Baylor College of Medicine, One Baylor Plaza, Room S670, M.S. BCM 295, Houston, TX 77030, Tel: 713-798-3981, Fax: 713-798-3946, tolias@bcm.edu.

learning and memory (Alvarez and Sabatini, 2007). Alternatively, aberrant spine morphogenesis is a hallmark of numerous neurodevelopmental, neuropsychiatric and neurodegenerative disorders (Newey et al., 2005). Thus, elucidating the mechanisms that regulate the formation and remodeling of excitatory synapses is important for understanding brain development and disease.

Rho GTPases play essential roles in the development and remodeling of excitatory synapses. In particular, Rac1 promotes spine and synapse formation, growth and maintenance (Govek et al., 2005). Rho GTPases function as molecular switches, cycling between an active GTP-bound and an inactive GDP-bound state. In their active state, they interact with effectors and stimulate signaling pathways that control cytoskeletal dynamics, membrane trafficking and gene expression (Govek et al., 2005). To function properly, Rho GTPases require precise spatio-temporal regulation (Pertz, 2010), and disruption of this regulation results in spine and synapse abnormalities and intellectual disabilities (Newey et al., 2005). Rho GTPases are activated by guanine nucleotide exchange factors (GEFs) and inhibited by GTPase-activating proteins (GAPs) (Tolias et al., 2011). However, little is known about how GEFs and GAPs act in concert to precisely regulate Rho GTPase signaling.

The Rac-GEF Tiam1 has emerged as a critical regulator of excitatory synapse development. Tiam1 is present in spines and couples synaptic receptors to Rac1 signaling pathways that control actin cytoskeletal remodeling (Duman et al., 2013; Lai et al., 2012; Tolias et al., 2005; Tolias et al., 2007; Zhang and Macara, 2006). Although Tiam1 function must be spatially and temporally restricted to properly control synaptogenesis (Duman et al., 2013; Zhang and Macara, 2006), the molecular basis of this regulation is unclear. Here, we identify the Rac-GAP Bcr as an important regulator of excitatory synapse development. We demonstrate that Bcr forms a GEF/GAP complex with Tiam1 that is essential for Rac1 signaling and synaptogenesis. Moreover, we show that EphB receptors utilize this complex to control synapse development. Like Tiam1, Bcr is critical for EphB-dependent spine formation. Unexpectedly, disruption of Bcr function converts EphB-mediated spine growth into retraction via Rac1-dependent EphB internalization. Bcr therefore serves to restrict Tiam1-induced Rac1 activation to an optimal range that promotes excitatory synapse formation and growth while preventing receptor endocytosis and synapse loss.

RESULTS

Interaction and colocalization of the Rac1 regulatory proteins Tiam1 and Bcr

To better understand the regulation of excitatory synapse development by Tiam1, we performed a yeast two-hybrid screen to identify Tiam1-interacting proteins. Our screen identified Bcr, a multi-domain Rac-GAP (Diekmann et al., 1991) (Figure S1A). By coimmunoprecipitation, we confirmed the Tiam1-Bcr association in both HEK293T cells (Figures 1A and S1B) and neurons (Figures 1B and S1C). To determine whether Tiam1 and Bcr interact at excitatory synapses, we assessed Tiam1 and Bcr colocalization in dendritic spines. Cultured rat hippocampal neurons expressing eGFP and low levels of Myc-tagged Bcr were fixed at 21 days in vitro (DIV) and costained for Myc and Tiam1. We found that Tiam1 colocalizes with Bcr in spines and dendrites (Figure 1C). Further, endogenous Bcr and Tiam1 were both enriched in the postsynaptic density (PSD) fraction of rat brain

extracts (Figure 1D), and they coimmunoprecipitated from purified synaptosomes (Figure 1E). Thus, Tiam1 and Bcr interact at synapses.

Bcr inhibits Tiam1-induced Rac1 signaling

An interaction between a Rac-specific GEF (Tiam1) and GAP (Bcr) is intriguing given their opposing effects on Rac1 activity. To determine whether Bcr inhibits Tiam1-induced Rac1 signaling, we expressed Flag-tagged Tiam1 in 293T cells with or without Myc-tagged Bcr constructs and assessed the effects on Rac1 activation and signaling. Coexpression of Bcr, but not a GAP-dead Bcr mutant (Bcr-GD), inhibited both Tiam1-induced Rac1 activation (Figure S1D) and autophosphorylation of Pak (Figures 1F and 1G), a Rac1 effector that regulates spine morphogenesis (Nikolic, 2008). To measure the effect of Bcr on Tiam1-mediated Rac1 signaling in neurons, we utilized the Förster resonance energy transfer (FRET) Rac1 activation biosensor RaichuEV-Rac1 (Komatsu et al., 2011). Bcr overexpression decreased Rac1 activation in dendrites and spines both basally and when coexpressed with Tiam1 (Figures 1H and 1I). Interestingly, Bcr-GD increased Rac1 activation to a similar extent as Tiam1, suggesting that this mutant functions as a dominant-negative (Figures 1H and 1I). These results indicate that Bcr antagonizes Tiam1 function by inhibiting Rac1.

Bcr negatively regulates spine development by inhibiting Rac1

The ability of Bcr to inhibit Rac1 in dendrites and spines suggests that it might control Rac1-dependent spine development. To investigate this possibility, we transfected 7 DIV rat hippocampal neurons with empty vector (pCMV-Myc) or plasmids encoding Myc-tagged Bcr or Bcr-GD in combination with eGFP to visualize neuronal morphology. Spines were analyzed at 21 DIV. Neurons overexpressing Bcr exhibited decreased spine density and increased filopodia density compared to control neurons (Figures 2A and 2B). In contrast, Bcr-GD increased spine density but had no effect on filopodia (Figures 2A and 2B). Bcr also increased protrusion length, whereas Bcr-GD decreased protrusion length but dramatically increased protrusion volume (Figures 2C and 2D). The Bcr constructs had similar, albeit more modest effects, when transfected into mature 20 DIV hippocampal neurons and analyzed at 28 DIV (Figure S1E and S1F). Thus, Bcr negatively regulates spine morphogenesis by inhibiting Rac1.

Loss of the Rac-GAPs Bcr and Abr causes defects in spine development *in vivo*

To determine whether Bcr functions similarly *in vivo*, we utilized mice lacking Bcr. $Bcr^{-/-}$ mice display abnormal stress responses, increased aggression, and impairments in LTP maintenance and memory (Oh et al., 2010; Voncken et al., 1998; Voncken et al., 1995). Mice lacking both Bcr and the highly related Rac-GAP Abr (Figure S2A) are more seriously impaired, exhibiting circling behavior, vestibular dysgenesis, cerebellar developmental defects, and abnormal inflammatory responses (Cunnick et al., 2009; Kaartinen et al., 2001; Kaartinen et al., 2002). The more severe phenotypes observed in the $Bcr^{-/-}Abr^{-/-}$ mice suggest that some functions of Bcr and Abr overlap. Abr may compensate for Bcr loss in neurons since Abr is present (though not enriched) at synapses (Figure 1D) (Oh et al., 2010), can interact with Tiam1 at synapses (Figure S2B), and inhibits spine maturation when

overexpressed in neurons (Figures S2D–G). Moreover, we found that Abr is upregulated (Figures 2E and 2F) and more enriched in the PSD fraction in the brains of $Bcr^{-/-}$ mice (Figure S2H). We therefore included mice lacking Abr in our analysis.

$Bcr^{-/-}$, $Abr^{-/-}$, and $Bcr^{-/-}Abr^{-/-}$ mice exhibit elevated Rac1 signaling in brain relative to WT mice (Figures 2G and 2H). To visualize spines *in vivo*, we crossed $Bcr^{-/-}$ and $Abr^{-/-}$ mice with *thy1*-YFP (line H) transgenic mice that express YFP in select neurons (Feng et al., 2000). Spine development was assessed in apical dendrites from YFP-positive CA1 pyramidal neurons in hippocampal sections obtained from postnatal day (P) 28 mice (Figure 2I). Both $Bcr^{-/-}$ and $Abr^{-/-}$ mice displayed increased spine density and small changes in spine size compared to WT mice (Figures 2I–L). Spine head area was slightly larger in $Bcr^{-/-}$ mice, whereas it was slightly smaller in $Abr^{-/-}$ mice (Figures 2I–L). In contrast, $Bcr^{-/-}Abr^{-/-}$ mice exhibited marked increases in both spine density and size (Figures 2I–L). In particular, they possessed a greater percentage of large spines compared to WT or single knockout mice (Figure 2L). Similar results were observed in $Bcr^{-/-}Abr^{+/-}$ mice (Figures S3A and S3B). These results suggest that Bcr and Abr restrict spinogenesis by inhibiting Rac1 activation *in vivo*.

To determine whether the higher spine density in mice lacking Bcr is due to an increase in spine formation and/or a decrease in spine elimination, we performed *in vivo* two-photon time-lapse imaging on pyramidal neuron apical dendrites in the somatosensory cortex of five-week-old YFP-expressing $Bcr^{+/+}Abr^{+/-}$ (control) and $Bcr^{-/-}Abr^{+/-}$ mice (Figure S3C). Individual dendritic segments were examined one hour apart to identify the formation of new spines (green arrows) and the elimination of existing spines (red arrows). Interestingly, we found that while the spine elimination rate was not decreased in the $Bcr^{-/-}Abr^{+/-}$ mice, the spine formation rate was significantly increased (Figure S3D). This result indicates that Bcr limits spine development *in vivo* by inhibiting spine formation.

Bcr restricts excitatory synapse development and function

To determine whether the exuberant spine phenotype caused by Bcr loss corresponds to an increase in excitatory synapses, we examined excitatory synapse development in neurons lacking Bcr function. Hippocampal neurons were isolated from P0 $Bcr^{-/-}Abr^{-/-}$ mice or control ($Bcr^{+/-}Abr^{+/-}$) littermates, which are indistinguishable from WT mice (data not shown). Neurons were cultured for 21 DIV and then stained for PSD-95 (post-synaptic marker) and VGLUT1 (pre-synaptic marker) to visualize excitatory synapses and phalloidin to visualize filamentous actin (F-actin) in spines (Figure 3A). Synapse density was determined by quantifying the number of colocalized PSD-95 and VGLUT1 puncta per unit area of dendrite. We observed an increase in excitatory synapse density in $Bcr^{-/-}Abr^{-/-}$ neurons relative to control neurons (Figure 3B). Overall staining intensity of PSD-95, VGLUT1, and F-actin also increased in neurons lacking Bcr and Abr (Figures 3C and 3D). Similar results were seen with $Bcr^{-/-}Abr^{+/-}$ cultured neurons (Figures S3E and S3F) and with rat hippocampal neurons expressing Bcr-GD (Figures 3E and 3F). Whole-cell patch-clamp measurements revealed that miniature excitatory postsynaptic currents (mEPSCs) in Bcr-GD-expressing hippocampal neurons have enhanced amplitude and frequency relative to control neurons (Figures 3G–I). Thus, neurons lacking Bcr function have more excitatory

synapses, which are larger, stronger, and contain more F-actin than control neurons, suggesting that Bcr restricts excitatory synaptogenesis by inhibiting Rac1.

A balance between Tiam1 and Bcr is required for proper spine development

Since Bcr interacts with Tiam1 and limits Tiam1-induced Rac1 signaling, we hypothesized that Bcr specifically opposes Tiam1's function at synapses, and that together Tiam1 and Bcr precisely regulate Rac1 activity during spinogenesis. To test this hypothesis, we examined whether the effects of loss of Bcr activity could be rescued by inhibiting Tiam1. We utilized two dominant-negative Tiam1 constructs: Tiam1-QK, a full-length Tiam1 mutant lacking Rac-GEF activity (Tolias et al., 2005), and PH-CC-Ex, the region of Tiam1 required for membrane recruitment (Mertens et al., 2003). Both constructs reduce spine density, likely by interfering with endogenous Tiam1 function (Figures 4A and 4B) (Tolias et al., 2005; Tolias et al., 2007). While Bcr-GD-expressing neurons possessed more and larger spines (Figures 4A–C), neurons expressing Bcr-GD and Tiam1-QK or PH-CC-Ex displayed spine density and size comparable to control neurons (Figures 4A–C). We confirmed these results using the small molecule inhibitor NSC23766, which specifically blocks Rac1 activation by Tiam1 (Figure S4) (Gao et al., 2004). Hippocampal slices prepared from P4 YFP-expressing WT and $Bcr^{-/-}Abr^{-/-}$ mice were cultured for 17 DIV and then treated with vehicle or NSC23766 for 1 hour. As before, $Bcr^{-/-}Abr^{-/-}$ neurons possessed more and larger spines than WT neurons (Figures 4D–F). NSC23766 reduced the density and size of spines to control levels (Figures 4D–F). These results indicate that the exuberant spine phenotype caused by loss of Bcr function is rescued by specifically inhibiting Tiam1, suggesting that a balance between Tiam1 and Bcr activities is essential for proper spine development.

Disruption of the Tiam1-Bcr complex augments Rac1 activation and spine development

We next asked whether the interaction between Tiam1 and Bcr is important for achieving the critical levels of Rac1 activity. To disrupt the Tiam1-Bcr complex, we needed to identify the domains that mediate their association. Using GST pull-down assays, we determined that bacterially-expressed Bcr constructs containing the N-terminal oligomerization and serine/threonine kinase domains (N-term) or the GAP domain (Figure 5A) interact with full-length Tiam1 expressed in COS7 cells (Figure 5B) and the Tiam1 PH-CC-Ex domain (Figure 5A) expressed in COS7 cells (Figure 5B) or bacteria (Figure 5C). The Tiam1 PH-CC-Ex domain binds with a four-fold higher affinity to the N-term domain of Bcr (K_d=7.10 × 10^{-8} M) than to Bcr's GAP domain (K_d=2.87 × 10^{-7} M) (Figure S5). These data demonstrate that the PH-CC-Ex domain of Tiam1 directly interacts with the N-term and GAP domains of Bcr.

Since N-term-Bcr bound with higher affinity to Tiam1, we tested whether it could disrupt the Tiam1-Bcr complex. Flag-Tiam1 coexpressed in 293T cells with Myc-Bcr in the presence or absence of Myc-N-term-Bcr was immunoprecipitated and assayed for Bcr association. N-term-Bcr effectively disrupted the interaction between full-length Tiam1 and Bcr (Figures 5D and 5E). To determine the effect of Tiam1-Bcr complex disruption on neuronal Rac1 activity, we measured Rac1 activation in vector- or N-term-Bcr-expressing neurons and found that it increased robustly in the dendrites and spines of neurons expressing N-term-Bcr (Figures 5F and 5G). This suggests that the Tiam1-Bcr interaction is required to limit Rac1 activity. To determine the effect of Tiam1-Bcr complex disruption on

spine development, we analyzed spine morphology in vector- or N-term-Bcr-expressing hippocampal neurons. Spine density and size increased in neurons overexpressing N-term-Bcr (Figures 5H–J). These results suggest that the interaction between Tiam1 and Bcr is important for maintaining the balance in their activities.

EphB receptors regulate the Tiam1-Bcr complex

Eph receptor tyrosine kinases regulate excitatory synapse development and plasticity (Klein, 2009). Following stimulation by their ephrin ligands, EphBs promote the formation and maturation of spines and synapses, whereas EphAs induce spine retraction and synapse loss (Klein, 2009). We previously established a critical role for Tiam1 in EphB-dependent spine formation (Tolias et al., 2007). To determine whether EphBs control spine morphogenesis by coordinately regulating the opposing functions of Tiam1 and Bcr, we first asked whether Bcr interacts with EphBs. Coimmunoprecipitation experiments in 293T cells revealed that like Tiam1, Bcr preferentially associates with EphB2 over EphA4 (Figure 6A). However, unlike Tiam1 (Tolias et al., 2007), the Bcr-EphB2 interaction is kinase-independent (Figure 6B). Interestingly, the same domains of Bcr (N-term and GAP domains) and Tiam1 (PH-CC-Ex) that bind to each other (Figure 5C) interact with EphB2 (Figure 6C) (Tolias et al., 2007), suggesting that these interactions may be competitive. Indeed, Tiam1 and Bcr compete with EphB2 for Bcr and Tiam1 binding, respectively (Figures 6D–G). Furthermore, eprhinB1-induced EphB activation in neurons reduces Tiam1-Bcr binding at the time of peak receptor activation (Figures S6A and S6B). These findings demonstrate that EphB interacts with both Bcr and Tiam1, and may transiently disrupt the Tiam1-Bcr complex when activated.

To investigate whether EphBs regulate the GEF and GAP activities of Tiam1 and Bcr, respectively, we stimulated 21 DIV hippocampal neurons with pre-clustered control Fc or ephrinB1-Fc (Figure 6H). Neurons were lysed and subjected to GEF or GAP pull-down assays using GST-Rac1-G15A (nucleotide-free Rac1 that binds to activated GEFs) or GST-Rac1-Q61L (constitutively-active Rac1 that binds to activated GAPs) (Garcia-Mata et al., 2006). EphrinB1 stimulation induced a transient increase in the amount of Tiam1 precipitating with GST-Rac1-G15A, peaking at around 10 minutes and returning to baseline by 60 minutes (Figures 6H and 6J). In contrast, the level of Bcr precipitating with GST-Rac1-Q61L initially decreased after ephrinB1 stimulation (Figures 6H and 6J). These alterations in Tiam1 and Bcr function correlate with a transient increase in Rac1 activity (Figures 6I and 6J), suggesting that EphBs control Rac1 activation by coordinately regulating the opposing activities of Tiam1 and Bcr. EphBs may regulate Tiam1 and Bcr function by modulating their phosphorylation state, since neuronal EphBs induce phosphorylation of Tiam1 (Tolias et al., 2007) and dephosphorylation of Bcr (Figures S6C–S6E) on sites known to cause GEF activation (Miyamoto et al., 2006) and GAP inhibition (Park et al., 2012), respectively.

To further characterize the role of Bcr in EphB-mediated Rac1 activation, we performed Rac1 activation assays on ephrinB1-stimulated rat hippocampal neurons expressing control vector or Bcr-GD (Figures 6K and 6L). Both control and Bcr-GD-expressing neurons displayed transient increases in Rac1 activity on dendrites and spines following ephrinB1

stimulation (Figures 6K and 6L). However, Rac1 activity was elevated throughout the entire time course of ephrinB1 stimulation in the Bcr-GD-expressing neurons (Figures 6K and 6L), suggesting that Bcr restricts the level of Rac1 activation in neurons.

Bcr is required for proper EphB-dependent excitatory synapse development

To investigate whether Bcr plays a role in EphB-dependent spine development, we performed morphometric analysis on 17 DIV organotypic hippocampal slice cultures from P4 YFP-expressing WT and $Bcr^{-/-}Abr^{-/-}$ mice stimulated with pre-clustered Fc (control), ephrinB1-Fc (to activate EphBs) or ephrinA1-Fc (to activate EphAs). As expected (Ethell et al., 2001; Henkemeyer et al., 2003; Murai et al., 2003; Penzes et al., 2003), ephrinB1 stimulation increased spine density, whereas ephrinA1 decreased spine density in WT neurons (Figures 7A and 7B). Neurons from $Bcr^{-/-}Abr^{-/-}$ slice cultures, which express an equivalent level of EphB (Figure S6J), possessed more spines under control conditions (Figures 7A and 7B). Surprisingly, we detected a dramatic decrease in spine density in $Bcr^{-/-}Abr^{-/-}$ neurons following ephrinB1 stimulation, comparable to that induced by ephrinA1 (Figures 7A and 7B). Thus, loss of Bcr/Abr converts EphB-mediated spine formation into spine retraction. Similar results were seen in rat hippocampal neurons expressing control vector or Bcr-GD. Fc-treated Bcr-GD-expressing neurons exhibited a greater spine density than Fc-treated control neurons (Figures 7C and 7D). EphrinB1 stimulation induced spinogenesis in control neurons, whereas it caused a decrease in spines on Bcr-GD-expressing neurons (Figures 7C and 7D). This stimulation-induced spine loss appears to be specific to EphB receptors, since BDNF stimulation of TrkB receptors caused no detectable change in spine density in Bcr-GD-expressing neurons (Figures S7A and S7B). Thus, disrupting Bcr function converts ephrinB-induced spinogenesis into spine loss, suggesting that Bcr is critical for EphB-dependent excitatory synapse development.

Since EphBs also regulate AMPA-type glutamate receptor localization (Henkemeyer et al., 2003; Kayser et al., 2006), we asked whether Bcr also plays a role in this process. Neurons expressing vector or Bcr-GD were stimulated with Fc or eprhinB1-Fc, and then subjected to live cell staining at 4 °C using an extracellular GluR1 antibody to detect surface AMPA receptors (Figure 7E). Total GluR1 staining was also analyzed in fixed and permeabilized neurons. Consistent with our spine and electrophysiology results, Bcr-GD-expressing neurons possessed a greater density of surface AMPA receptor puncta than control neurons (Figures 7E and 7F). EphrinB1 increased AMPA receptor surface levels in control neurons, whereas it caused AMPA receptor internalization in Bcr-GD-expressing neurons (Figures 7E and 7F). Total AMPA receptor levels were not altered (data not shown). Bcr is therefore important for regulating AMPA receptor localization, both basally and in response to EphB activation.

Bcr regulates ephrinB-induced spine formation by restricting Rac-dependent EphB internalization

To determine how Bcr influences EphB-dependent excitatory synapse development, we investigated the mechanism by which ephrinB stimulation induces spine loss in the absence of Bcr function. Theoretically, the high-affinity intercellular interactions between Ephs and ephrins should promote cell-cell adhesion, but they often cause contact-mediated repulsion

(Pasquale, 2005). To convert an adhesive interaction into repulsion, Eph-ephrin complexes must be removed from the cell surface, in part through bi-directional endocytosis (Egea and Klein, 2007; Marston et al., 2003; Zimmer et al., 2003). Endocytosis of Eph-ephrin complexes and subsequent repulsion requires Rac-dependent actin remodeling (Cowan et al., 2005; Marston et al., 2003; Yoo et al., 2011; Yoo et al., 2010). As Rac1 signaling is elevated in neurons lacking Bcr function (Figures 2H and 6H), we hypothesized that ephrinB induces axon-dendrite repulsion and spine retraction in these cells by triggering Rac-dependent EphB endocytosis. To investigate this possibility, we compared the effects of ephrinB stimulation on EphB internalization in WT versus $Bcr^{-/-}Abr^{-/-}$ neurons. 21 DIV dissociated hippocampal neurons from P0 WT or $Bcr^{-/-}Abr^{-/-}$ mice were stimulated with pre-clustered Fc or ephrinB1-Fc and subjected to live cell staining at 4°C to detect surface EphB-ephrinB clusters (Figure 7G, red puncta in overlay). Following fixation and permeabilization, neurons were stained for the remaining EphB-ephrinB clusters (Figure 7G). Internalized EphB receptor clusters were identified by subtracting surface EphB-ephrinB staining from permeabilized EphB-ephrinB staining (Figure 7G, green puncta in overlay). This analysis revealed that ephrinB stimulation dramatically increased EphB internalization in $Bcr^{-/-}Abr^{-/-}$ neurons but not in WT neurons, which display low levels of EphB internalization (Figure 7H). These results suggest that Bcr/Abr restrict EphB receptor endocytosis.

To determine whether Rac-mediated EphB endocytosis converts ephrinB-stimulated spine growth into retraction in $Bcr^{-/-}Abr^{-/-}$ neurons, we blocked EphB internalization with the clathrin-mediated endocytosis inhibitor monodansylcadaverine (MDC) (Heerssen et al., 2004; Shieh et al., 2011) or the Tiam1 inhibitor NSC23766. Dissociated hippocampal neurons from WT or $Bcr^{-/-}Abr^{-/-}$ mice were pretreated with vehicle (DMSO), MDC, or NSC23766 and then stimulated with pre-clustered Fc or ephrinB1-Fc for 30 min. Neurons then underwent EphB internalized cluster analysis and phalloidin staining for spine analysis. Pretreatment with MDC or NSC23766 dramatically decreased ephrinB-induced EphB internalization in $Bcr^{-/-}Abr^{-/-}$ neurons (Figure 7I). Importantly, MDC treatment also inhibited ephrinB-induced spine retraction in $Bcr^{-/-}Abr^{-/-}$ neurons, whereas it had no effect on ephrinB-induced spinogenesis in WT neurons (Figure 7J). This result suggests that EphB endocytosis is required for ephrinB-induced spine retraction in $Bcr^{-/-}Abr^{-/-}$ neurons, but is not necessary for ephrinB-induced spinogenesis in WT neurons. In contrast, NSC23766 blocked both ephrinB-induced spine retraction in $Bcr^{-/-}Abr^{-/-}$ neurons and ephrinB-induced spinogenesis in WT neurons (Figure 7J), suggesting that active Rac1 is required for spine development, but can also drive spine retraction in conditions of hyperactivity. Similar results were observed in rat hippocampal neurons lacking Bcr function. EphrinB1-induced spine loss in Bcr-GD-expressing neurons was blocked by pretreatment with dynasore (Figures S7C and S7D), a small molecule inhibitor of dynamin-dependent endocytosis (Kirchhausen et al., 2008). Together, these results confirm that EphB activation induces spine loss in neurons lacking Bcr function due to Rac-dependent EphB internalization. Bcr may therefore normally serve to restrict active Rac1 levels to within an optimal range that promotes appropriate excitatory synapse formation and growth while preventing receptor internalization and excessive spine remodeling.

DISCUSSION

Here, we demonstrate that a complex composed of a Rac-GEF (Tiam1) and a Rac-GAP (Bcr) coordinately regulates spine and synapse development. We base this conclusion on our findings that i) Bcr interacts with Tiam1 at synapses, ii) enhancing Bcr function through overexpression reduces spine size and density, iii) inhibiting Bcr function through genetic deletion or dominant-negative mutants increases the size and density of spines and the size, density and strength of excitatory synapses, iv) inhibition of Tiam1 function rescues the synaptic defects induced by reduced Bcr function, and v) disruption of the Tiam1-Bcr interaction causes excessive Rac1 activity and spine development. Notably, EphBs utilize the Tiam1-Bcr complex to control spine morphogenesis. Activated EphBs interact with Tiam1 and Bcr and regulate their respective GEF and GAP activities. Tiam1 subsequently mediates EphB-induced Rac1 activation and spine formation (Tolias et al., 2007), whereas Bcr restricts Rac1 activation, preventing EphB and AMPA receptor internalization and spine loss. These data provide strong evidence that a GEF/GAP complex dynamically regulates synaptic Rac1 signaling.

Bcr$^{-/-}$ mice exhibit impairments in LTP maintenance and spatial and object recognition memory (Oh et al., 2010). However, only a slight increase in spine density was observed in these mice, and no change in spine size or excitatory synaptic transmission was detected (Oh et al., 2010). *Bcr*$^{-/-}$ mice may lack significant synaptic defects due to compensation by Abr (Cho et al., 2007; Kaartinen et al., 2001), which is upregulated and more enriched in the PSD in the brains of mice lacking Bcr. To fully understand Bcr's role in excitatory synapse development, it is necessary to examine the effects of loss of Bcr in the presence or absence of Abr. Indeed, we found striking increases in the size and density of spines and synapses in *Bcr*$^{-/-}$*Abr*$^{-/-}$ and *Bcr*$^{-/-}$*Abr*$^{+/-}$ mice compared to control littermates. We also found that spines in Bcr-deficient mice undergo more rapid remodeling than those in control mice, which is likely mediated by excessive Rac1-dependent actin cytoskeletal reorganization. This increased spine remodeling could further explain why *Bcr*$^{-/-}$ mice exhibit a defect in LTP maintenance.

Though Bcr and Abr share some overlapping functions at synapses, we do not believe they play identical roles. For instance, we found that CA1 hippocampal neurons from *Bcr*$^{-/-}$ mice display a small increase in spine size, whereas neurons from *Abr*$^{-/-}$ mice exhibit a small decrease. Furthermore, overexpression of Bcr induces substantial spine loss, whereas Abr promotes the formation of immature spines. Bcr is also more enriched at synapses than Abr, and it preferentially interacts with Tiam1. Interestingly, in adult brain we found that Abr preferentially interacts with Kalirin-7 (Figure S2D), another Rac-GEF essential for synapse development and plasticity (Penzes and Jones, 2008). Abr and Kalirin-7 may therefore form a unique GEF/GAP complex, which, based on their expression profiles (Oh et al., 2010; Penzes et al., 2008), could regulate Rac-dependent processes later in development. This finding argues that GEF/GAP complex formation is a general phenomenon extending beyond Tiam1 and Bcr.

A GEF/GAP interaction might seem counterproductive, since they oppose one another functionally. However, it is clear that proper on-off cycling of Rac1 is important since

constitutively-active and dominant-negative Rac1 mutants both perturb Rac-driven processes such as cell migration and spine development (Luo et al., 1996; Nakayama et al., 2000; Spiering and Hodgson, 2011). Formation of a Rac-specific GEF/GAP complex may provide an efficient mechanism for dynamically regulating Rac1 activity, as predicted (Goryachev and Pokhilko, 2006). A GEF/GAP complex could also help spatially and temporally regulate Rac1 activity. Indeed, we recently found that Bcr interacts with the Tiam1-associated Par complex and controls polarized cell migration by locally restricting Rac1 and PKCζ activity at the leading edge (Narayanan et al., 2013).

The finding that EphB receptors interact with Tiam1 and Bcr and regulate their activities and association suggests that EphBs control Rac1 signaling by modulating the Tiam1-Bcr complex. Under basal conditions, Tiam1 and Bcr form a strong complex in neurons that may be associated with EphBs via Bcr. EphB activation triggers the phosphorylation of Tiam1 (Tolias et al., 2007) and the dephosphorylation of Bcr. Phosphorylation of Tiam1 enhances its recruitment to EphB complexes and its Rac-GEF activity (Tolias et al., 2005; Miyamoto et al., 2006; Tolias et al., 2007), whereas dephosphorylation of Bcr may reduce its binding to Tiam1 and its Rac-GAP activity (Park et al., 2012). This coordinated regulation of Tiam1 and Bcr likely contributes to the transient increase in Rac1 activation required for EphB-dependent spine growth. Further investigation is required to determine the precise mechanism by which EphBs regulate the Tiam1-Bcr complex. In the absence of Bcr function, Rac1 activity is basally high, resulting in a greater number of large spines. Under these conditions, ephrinB induces excessive Rac1 activation, EphB and AMPA receptor internalization, and spine retraction. Since inhibition of either Rac1 activation or endocytosis blocks ephrinB-induced spine loss, we conclude that Rac-dependent EphB internalization is responsible for converting excitatory synapse development into synapse elimination. Eph internalization is known to convert adhesive interactions between Ephs and ephrins into repulsion during axon guidance and cell sorting (Pitulescu and Adams, 2010). By binding to EphBs and restricting local Rac1 activity, Bcr may stabilize EphBs on the cell surface at synapses, enabling activated EphBs to promote synaptogenesis and AMPA receptor surface expression rather than axon-dendrite repulsion and synapse loss. It will be interesting to determine whether other Tiam1-interacting receptors including NMDA receptors, TrkB receptors, and the adhesion-GPCR BAI1 coordinately regulate the Tiam1-Bcr complex (Duman et al., 2013; Lai et al., 2012; Tolias et al., 2005; Tolias et al., 2007).

Altered Rac1 signaling is associated with a variety of brain disorders, suggesting that proper Rac1 signaling is required for normal cognitive function (Newey et al., 2005; Ramakers, 2002). However, despite its importance, little is known about how Rac1 signaling is dynamically regulated at synapses. In this study, we characterized a complex composed of two opposing Rac1 regulatory proteins, Bcr and Tiam1, and demonstrated that they play essential roles in controlling excitatory synapse development by providing precise regulation of Rac1 activity. Further study elucidating the roles of this and other Rac1 regulatory complexes in synapse development and function should enhance our understanding of normal brain development and provide new insight into how disruptions in Rac1 signaling give rise to cognitive disorders.

EXPERIMENTAL PROCEDURES

DNA Constructs, Antibodies and Drugs

Details can be found in the Supplemental Information.

Mice, Cell Culture, and Transfections

Bcr$^{-/-}$ and *Thy1*-YFP (line H) mice were obtained from Jackson Laboratory (Bar Harbor, Maine) and *Abr*$^{-/-}$ mice were generously provided by Dr. Nora Heisterkamp (Children's Hospital LosAngeles, USC). For cell culture and transfection conditions, see the Supplemental data.

Immunoprecipitations, GST pull-down assay, and Western Blot Analysis

For details, see the Supplemental data.

Preparation of Aggregated Ephrin-Fc Fusion Proteins

EphrinB1-Fc (eB1), ephrinA1-Fc (eA1) (R&D Systems) and control Fc (Jackson ImmunoResearch Labs) were preclustered with 100 μg/ml goat α-human IgG Fcγ antibody (Jackson ImmunoResearch Labs) at 50 μg/ml at 25°C for 1 h and then used at final concentration of 2.5 μg/ml.

Immunocytochemistry

For details, see the Supplemental data.

FRET assay

Rat hippocampal neurons were cultured in phenol red-free Neurobasal medium (Invitrogen) supplemented with B27 (Gibco BRL), 2 mM glutamine and penicillin/streptomycin (100 U/ml and 100 μg/ml, respectively) and transfected on 7 DIV with the RaichuEV-Rac1 probe (Komatsu et al., 2011) alone or with Tiam1 and/or Bcr reagents. At 17 DIV, neurons expressing moderate levels of the RaichuEV-Rac1 probe were imaged with or without eB1 stimulation using a Leica TCS SP2 scanning confocal microscope with a 63x oil immersion objective (2x digital zoom) at 1024×1024 pixel resolution. Images were obtained with the following settings; FRET: Ex 458 nm/Em 530–600 nm, CFP: Ex 458 nm/Em 470–500 nm, YFP: Ex 514 nm/Em 530–600 nm. After acquisition, pixel-by-pixel FRET was calculated and images were created using the ImageJ plug-in PixFRET (Feige et al., 2005) and represented in an intensity-modulated display mode. All FRET experiments were conducted at least three independent times.

Receptor Endocytosis Assays

To analyze EphB internalization, 21 DIV mouse hippocampal neurons were incubated with preclustered Fc or eB1 for 30 min at 37°C. Before live staining, surface receptors were labeled with unclustered eB1 for 10 min at 37°C. Cells were washed 3x with PBS and EphB-eB1 complexes were live-labeled with a Cy3-goat α-human Fc antibody for 30 min at 4°C. After washing 3x with PBS, cells were fixed with 4% PFA/4% sucrose for 10 min at 25°C and then blocked/ permeabilized with 5% BSA, 15% goat serum and 0.3% Triton

X-100 in PBS for 30 min. The remaining EphB-eB1 complexes were stained with a Cy5-goat α-human Fc antibody at 25°C for 30 min (Cowan et al., 2005; Deininger et al., 2008). Confocal images were then acquired using fixed parameters, and custom ImageJ macros were used to quantify EphB-eB1 staining intensity. Internalized EphB receptors were determined by subtracting surface staining from permeablized EphB complex staining using Image Calculator on ImageJ, and total EphB staining was determined as the sum of surface and internalized EphB complexes. The data were plotted as the ratio of internalized over total EphB complexes.

For surface AMPA receptor labeling, live cultured neurons were incubated with anti-GluR1 antibody (N-term, Millipore) for 30 min at 4°C and washed 3x with PBS, and then fixed with 4% PFA/4% sucrose. Fixed neurons were then stained with an anti-mouse Cy3 secondary antibody. For total AMPA receptor staining, neurons were fixed with 100% methanol at −20°C for 10 min and blocked/permeabilized with 5% BSA, 15% goat serum and 0.3% Triton X-100 in PBS for 1 hr at 25°C. Anti-GluR1 (C-term, Millipore) antibodies were incubated at 4°C overnight, and then anti-rabbit Cy3 secondary antibodies were applied for 1 hr at 25°C. For analysis, images were acquired using fixed parameters, and surface and total GluR1 puncta densities on Myc-expressing neurons were quantified using custom macros from ImageJ.

Imaging and Analysis

Neurons from dissociated hippocampal cultures, organotypic slice cultures, and floating brain sections were imaged using the confocal system described above. Z-series of 6–10 images taken at 0.4 μm intervals (cultured neurons) or 16–18 images taken at 0.12 μm intervals (slice cultures and floating sections) were generated for each dendritic section. For each experiment, 8–10 neurons/condition were imaged and analyzed blinded and this was repeated at least 3 independent times. Imaris (Bitplane Scientific Software) was used to analyze 3-D spine images. Approximately 100 μm of dendrite was chosen per neuron, and the number of spines (visualized by eGFP for cultured rat neurons and phalloidin for cultured mouse neurons) was counted and the length and volume of dendritic protrusions were measured using Imaris. Dendritic protrusions were classified as filopodia if their lengths exceeded 2 μm and they lacked spine heads. For spine analysis of YFP-labeled neurons from organotypic cultures or brain sections, third and fourth order apical dendrites were imaged. Spines were scored only if they exhibited a neck and a mushroom- or thin-shaped head (predominant protrusions observed in P28 mouse brain sections and 11 DIV slice cultures). Spines were quantified from confocal images of dendritic segments traced with the Neurolucida/ NeuroExplorer software (MBF Bioscience). To assess synaptic and F-actin staining, neurons were imaged using the same exposure parameters for the different genotypes, and the images analyzed using ImageJ software (NIH). For synaptic density analysis, overlapping PSD-95 and VGLUT1 puncta masked by phalloidin staining were quantified and divided by dendritic area. Mean pixel intensities of phalloidin, PSD-95 and VGLUT1 staining on spines were also measured and adjusted for local background.

Electrophysiology

Electrophysiology was performed using standard methods (see Supplementary Information).

Statistical Analysis

Data were expressed as means ± standard error and statistically analyzed using KaleidaGraph (Synergy Software). Statistical significance was determined using Student's t-test for comparison between two independent groups and ANOVA with Tukey's Post Hoc test for multiple group comparisons unless otherwise stated. $p<0.05$ was considered statistically significant.

Supplementary Material

Refer to Web version on PubMed Central for supplementary material.

Acknowledgments

We thank N. Heisterkemp for generously providing $Abr^{-/-}$ mice and Abr cDNA constructs and M. Matsuda for the RaichuEV-Rac1 construct. We greatly appreciate C. Peters and N. Lee for providing technical advice and assistance, respectively. We also thank M. Greenberg, H. Zoghbi, M. Rasband, and J. Glaven for helpful comments. This work was supported by the National Institute of Neurological Disorders and Stroke grant RO1NS062829 (K.F.T.), Mission Connect-TIRR Foundation (K.F.T.), the National Institute of Mental Health grant K01MH089112 (J.G.D.), and the Eunice Kennedy Shriver National Institute Of Child Health & Human Development grant P30HD024064.

References

Alvarez VA, Sabatini BL. Anatomical and physiological plasticity of dendritic spines. Annu Rev Neurosci. 2007; 30:79–97. [PubMed: 17280523]

Cho YJ, Cunnick JM, Yi SJ, Kaartinen V, Groffen J, Heisterkamp N. Abr and Bcr, two homologous Rac GTPase-activating proteins, control multiple cellular functions of murine macrophages. Mol Cell Biol. 2007; 27:899–911. [PubMed: 17116687]

Cowan CW, Shao YR, Sahin M, Shamah SM, Lin MZ, Greer PL, Gao S, Griffith EC, Brugge JS, Greenberg ME. Vav family GEFs link activated Ephs to endocytosis and axon guidance. Neuron. 2005; 46:205–217. [PubMed: 15848800]

Cunnick JM, Schmidhuber S, Chen G, Yu M, Yi SJ, Cho YJ, Kaartinen V, Minoo P, Warburton D, Groffen J, et al. Bcr and Abr cooperate in negatively regulating acute inflammatory responses. Mol Cell Biol. 2009; 29:5742–5750. [PubMed: 19703997]

Deininger K, Eder M, Kramer ER, Zieglgansberger W, Dodt HU, Dornmair K, Colicelli J, Klein R. The Rab5 guanylate exchange factor Rin1 regulates endocytosis of the EphA4 receptor in mature excitatory neurons. Proc Natl Acad Sci U S A. 2008; 105:12539–12544. [PubMed: 18723684]

Diekmann D, Brill S, Garrett MD, Totty N, Hsuan J, Monfries C, Hall C, Lim L, Hall A. Bcr encodes a GTPase-activating protein for p21rac. Nature. 1991; 351:400–402. [PubMed: 1903516]

Duman JG, Tzeng CP, Tu YK, Munjal T, Schwechter B, Ho TS, Tolias KF. The adhesion-GPCR BAI1 regulates synaptogenesis by controlling the recruitment of the Par3/Tiam1 polarity complex to synaptic sites. J Neurosci. 2013; 33:6964–6978. [PubMed: 23595754]

Egea J, Klein R. Bidirectional Eph-ephrin signaling during axon guidance. Trends Cell Biol. 2007; 17:230–238. [PubMed: 17420126]

Ethell IM, Irie F, Kalo MS, Couchman JR, Pasquale EB, Yamaguchi Y. EphB/syndecan-2 signaling in dendritic spine morphogenesis. Neuron. 2001; 31:1001–1013. [PubMed: 11580899]

Feige JN, Sage D, Wahli W, Desvergne B, Gelman L. PixFRET, an ImageJ plug-in for FRET calculation that can accommodate variations in spectral bleed-throughs. Microsc Res Tech. 2005; 68:51–58. [PubMed: 16208719]

Feng G, Mellor RH, Bernstein M, Keller-Peck C, Nguyen QT, Wallace M, Nerbonne JM, Lichtman JW, Sanes JR. Imaging neuronal subsets in transgenic mice expressing multiple spectral variants of GFP. Neuron. 2000; 28:41–51. [PubMed: 11086982]

Gao Y, Dickerson JB, Guo F, Zheng J, Zheng Y. Rational design and characterization of a Rac GTPase-specific small molecule inhibitor. Proc Natl Acad Sci U S A. 2004; 101:7618–7623. [PubMed: 15128949]

Garcia-Mata R, Wennerberg K, Arthur WT, Noren NK, Ellerbroek SM, Burridge K. Analysis of activated GAPs and GEFs in cell lysates. Methods Enzymol. 2006; 406:425–437. [PubMed: 16472675]

Goryachev AB, Pokhilko AV. Computational model explains high activity and rapid cycling of Rho GTPases within protein complexes. PLoS Comput Biol. 2006; 2:e172. [PubMed: 17140284]

Govek EE, Newey SE, Van Aelst L. The role of the Rho GTPases in neuronal development. Genes Dev. 2005; 19:1–49. [PubMed: 15630019]

Heerssen HM, Pazyra MF, Segal RA. Dynein motors transport activated Trks to promote survival of target-dependent neurons. Nat Neurosci. 2004; 7:596–604. [PubMed: 15122257]

Henkemeyer M, Itkis OS, Ngo M, Hickmott PW, Ethell IM. Multiple EphB receptor tyrosine kinases shape dendritic spines in the hippocampus. J Cell Biol. 2003; 163:1313–1326. [PubMed: 14691139]

Kaartinen V, Gonzalez-Gomez I, Voncken JW, Haataja L, Faure E, Nagy A, Groffen J, Heisterkamp N. Abnormal function of astroglia lacking Abr and Bcr RacGAPs. Development. 2001; 128:4217–4227. [PubMed: 11684658]

Kaartinen V, Nagy A, Gonzalez-Gomez I, Groffen J, Heisterkamp N. Vestibular dysgenesis in mice lacking Abr and Bcr Cdc42/RacGAPs. Dev Dyn. 2002; 223:517–525. [PubMed: 11921339]

Kayser MS, McClelland AC, Hughes EG, Dalva MB. Intracellular and trans-synaptic regulation of glutamatergic synaptogenesis by EphB receptors. J Neurosci. 2006; 26:12152–12164. [PubMed: 17122040]

Kirchhausen T, Macia E, Pelish HE. Use of dynasore, the small molecule inhibitor of dynamin, in the regulation of endocytosis. Methods Enzymol. 2008; 438:77–93. [PubMed: 18413242]

Klein R. Bidirectional modulation of synaptic functions by Eph/ephrin signaling. Nat Neurosci. 2009; 12:15–20. [PubMed: 19029886]

Komatsu N, Aoki K, Yamada M, Yukinaga H, Fujita Y, Kamioka Y, Matsuda M. Development of an optimized backbone of FRET biosensors for kinases and GTPases. Mol Biol Cell. 2011; 22:4647–4656. [PubMed: 21976697]

Lai KO, Wong AS, Cheung MC, Xu P, Liang Z, Lok KC, Xie H, Palko ME, Yung WH, Tessarollo L, et al. TrkB phosphorylation by Cdk5 is required for activity-dependent structural plasticity and spatial memory. Nat Neurosci. 2012; 15:1506–1515. [PubMed: 23064382]

Luo L, Hensch TK, Ackerman L, Barbel S, Jan LY, Jan YN. Differential effects of the Rac GTPase on Purkinje cell axons and dendritic trunks and spines. Nature. 1996; 379:837–840. [PubMed: 8587609]

Marston DJ, Dickinson S, Nobes CD. Rac-dependent trans-endocytosis of ephrinBs regulates Eph-ephrin contact repulsion. Nat Cell Biol. 2003; 5:879–888. [PubMed: 12973357]

Mertens AE, Roovers RC, Collard JG. Regulation of Tiam1-Rac signalling. FEBS Lett. 2003; 546:11–16. [PubMed: 12829230]

Miyamoto Y, Yamauchi J, Tanoue A, Wu C, Mobley WC. TrkB binds and tyrosine-phosphorylates Tiam1, leading to activation of Rac1 and induction of changes in cellular morphology. Proc Natl Acad Sci U S A. 2006; 103:10444–10449. [PubMed: 16801538]

Murai KK, Nguyen LN, Irie F, Yamaguchi Y, Pasquale EB. Control of hippocampal dendritic spine morphology through ephrin-A3/EphA4 signaling. Nat Neurosci. 2003; 6:153–160. [PubMed: 12496762]

Nakayama AY, Harms MB, Luo L. Small GTPases Rac and Rho in the maintenance of dendritic spines and branches in hippocampal pyramidal neurons. J Neurosci. 2000; 20:5329–5338. [PubMed: 10884317]

Narayanan AS, Reyes SB, Um K, McCarty JH, Tolias KF. The Rac-GAP Bcr is a novel regulator of the Par complex that controls cell polarity. Mol Biol Cell. 2013; 24:3857–3868. [PubMed: 24152735]

Newey SE, Velamoor V, Govek EE, Van Aelst L. Rho GTPases, dendritic structure, and mental retardation. J Neurobiol. 2005; 64:58–74. [PubMed: 15884002]

Nikolic M. The Pak1 kinase: an important regulator of neuronal morphology and function in the developing forebrain. Mol Neurobiol. 2008; 37:187–202. [PubMed: 18649038]

Oh D, Han S, Seo J, Lee JR, Choi J, Groffen J, Kim K, Cho YS, Choi HS, Shin H, et al. Regulation of synaptic Rac1 activity, long-term potentiation maintenance, and learning and memory by BCR and ABR Rac GTPase-activating proteins. J Neurosci. 2010; 30:14134–14144. [PubMed: 20962234]

Park AR, Oh D, Lim SH, Choi J, Moon J, Yu DY, Park SG, Heisterkamp N, Kim E, Myung PK, et al. Regulation of dendritic arborization by BCR Rac1 GTPase-activating protein, a substrate of PTPRT. J Cell Sci. 2012; 125:4518–4531. [PubMed: 22767509]

Pasquale EB. Eph receptor signalling casts a wide net on cell behaviour. Nat Rev Mol Cell Biol. 2005; 6:462–475. [PubMed: 15928710]

Penzes P, Beeser A, Chernoff J, Schiller MR, Eipper BA, Mains RE, Huganir RL. Rapid induction of dendritic spine morphogenesis by trans-synaptic ephrinB-EphB receptor activation of the Rho-GEF kalirin. Neuron. 2003; 37:263–274. [PubMed: 12546821]

Penzes P, Cahill ME, Jones KA, Srivastava DP. Convergent CaMK and RacGEF signals control dendritic structure and function. Trends Cell Biol. 2008; 18:405–413. [PubMed: 18701290]

Penzes P, Jones KA. Dendritic spine dynamics--a key role for kalirin-7. Trends Neurosci. 2008; 31:419–427. [PubMed: 18597863]

Pertz O. Spatio-temporal Rho GTPase signaling - where are we now? J Cell Sci. 2010; 123:1841–1850. [PubMed: 20484664]

Pitulescu ME, Adams RH. Eph/ephrin molecules--a hub for signaling and endocytosis. Genes Dev. 2010; 24:2480–2492. [PubMed: 21078817]

Ramakers GJ. Rho proteins, mental retardation and the cellular basis of cognition. Trends Neurosci. 2002; 25:191–199. [PubMed: 11998687]

Shieh JC, Schaar BT, Srinivasan K, Brodsky FM, McConnell SK. Endocytosis regulates cell soma translocation and the distribution of adhesion proteins in migrating neurons. PLoS ONE. 2011; 6:e17802. [PubMed: 21445347]

Spiering D, Hodgson L. Dynamics of the Rho-family small GTPases in actin regulation and motility. Cell Adh Migr. 2011; 5:170–180. [PubMed: 21178402]

Tolias KF, Bikoff JB, Burette A, Paradis S, Harrar D, Tavazoie S, Weinberg RJ, Greenberg ME. The Rac1-GEF Tiam1 couples the NMDA receptor to the activity-dependent development of dendritic arbors and spines. Neuron. 2005; 45:525–538. [PubMed: 15721239]

Tolias KF, Bikoff JB, Kane CG, Tolias CS, Hu L, Greenberg ME. The Rac1 guanine nucleotide exchange factor Tiam1 mediates EphB receptor-dependent dendritic spine development. Proc Natl Acad Sci U S A. 2007; 104:7265–7270. [PubMed: 17440041]

Tolias KF, Duman JG, Um K. Control of synapse development and plasticity by Rho GTPase regulatory proteins. Prog Neurobiol. 2011; 94:133–148. [PubMed: 21530608]

Voncken JW, Baram TZ, Gonzales-Gomez II, van Schaick H, Shih JC, Chen K, Groffen J, Heisterkamp N. Abnormal stress response and increased fighting behavior in mice lacking the bcr gene product. Int J Mol Med. 1998; 2:577–583. [PubMed: 9858655]

Voncken JW, van Schaick H, Kaartinen V, Deemer K, Coates T, Landing B, Pattengale P, Dorseuil O, Bokoch GM, Groffen J, et al. Increased neutrophil respiratory burst in bcr-null mutants. Cell. 1995; 80:719–728. [PubMed: 7889565]

Yoo S, Kim Y, Noh H, Lee H, Park E, Park S. Endocytosis of EphA receptors is essential for the proper development of the retinocollicular topographic map. Embo J. 2011; 30:1593–1607. [PubMed: 21343910]

Yoo S, Shin J, Park S. EphA8-ephrinA5 signaling and clathrin-mediated endocytosis is regulated by Tiam-1, a Rac-specific guanine nucleotide exchange factor. Mol Cells. 2010; 29:603–609. [PubMed: 20496116]

Zhang H, Macara IG. The polarity protein PAR-3 and TIAM1 cooperate in dendritic spine morphogenesis. Nat Cell Biol. 2006; 8:227–237. [PubMed: 16474385]

Zimmer M, Palmer A, Kohler J, Klein R. EphB-ephrinB bi-directional endocytosis terminates adhesion allowing contact mediated repulsion. Nat Cell Biol. 2003; 5:869–878. [PubMed: 12973358]

Highlights

- The Rac-GAP Bcr is a critical regulator of synapse and spine development.
- Tiam1 and Bcr form a GEF/GAP complex, which precisely regulates Rac1 signaling.
- EphB receptors utilize this GEF/GAP complex to promote excitatory synaptogenesis.
- Bcr restricts Rac1-mediated EphB endocytosis, enabling Tiam1-induced spine growth.

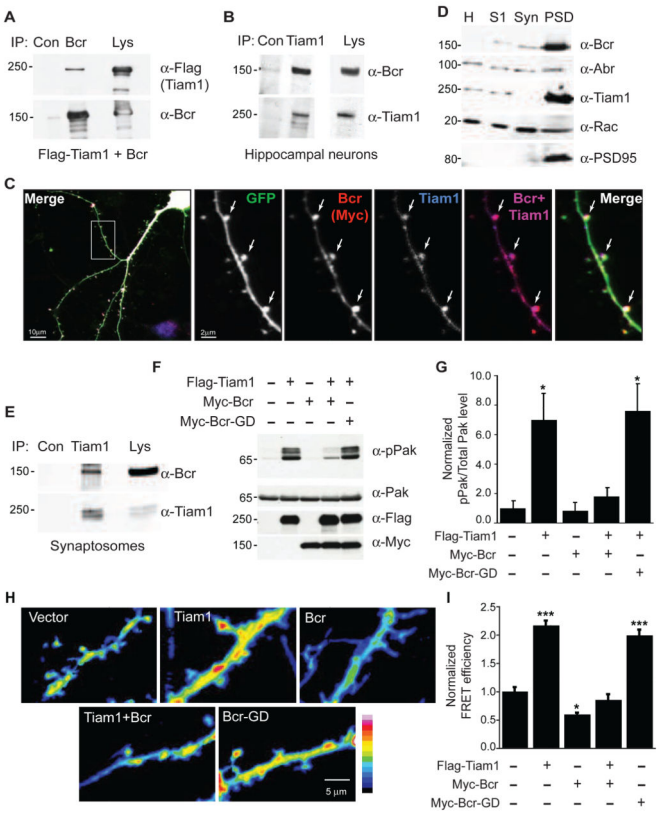

Figure 1. Bcr interacts with Tiam1 and blocks Tiam1-induced Rac1 signaling

(A) Lysates from HEK293T cells expressing Flag-Tiam1 and Bcr were immunoprecipitated (IP) with anti-Bcr or control (Con) IgG antibodies, and then immunoblotted with anti-Flag or anti-Bcr antibodies. Lysates (Lys) were also probed to confirm protein expression.

(B) Lysates from 14 DIV rat hippocampal neurons were immunoprecipitated with anti-Tiam1 or control antibodies, and then immunoblotted with anti-Bcr or anti-Tiam1 antibodies.

(C) 21 DIV hippocampal neurons expressing eGFP and low levels of Myc-Bcr were fixed and stained for Tiam1 and Myc (blue and red, respectively, in overlay images). Arrows indicate Tiam1 and Bcr colocalization in spines.

(D) Bcr and Tiam1 are enriched in the postsynaptic density (PSD) fraction of P18 rat brain extracts. Brain homogenate (H) was separated into soluble (S1), synaptosome (Syn) and PSD fractions, and then immunoblotted with antibodies against Bcr, Abr, Tiam1, Rac, or PSD95. Unlike Bcr and Tiam1, Abr is evenly distributed in all fractions.

(E) Synaptosomal fractions from P18 rat brain were immunoprecipitated with anti-Tiam1 or control IgG antibodies, and then immunoblotted with anti-Bcr or anti-Tiam1 antibodies.

(F and G) Lysates from 293T cells expressing Flag-Tiam1 alone or with Myc-Bcr or Myc-Bcr-GD (GAP-dead) were immunoblotted with anti-pPak antibodies (F) to assess Rac-dependent Pak phosphorylation. Levels of Pak, Flag-Tiam1, and Myc-Bcr were confirmed by immunoblotting.

(G) Quantification of normalized phosphorylated Pak levels, represented as a ratio of pPak over Pak intensity. N=3.

(H and I) Dissociated rat hippocampal neurons expressing the Rac1 activation biosensor RaichuEV-Rac1 with vector, Flag-Tiam1, Myc-Bcr, or Myc-Bcr-GD were live-imaged at 17 DIV. Representative FRET images are shown in the intensity-modulated display mode (H), and represented as relative mean FRET efficiency (I). n=27 neurons (vector); n=17 (Tiam1); n=12 (Bcr); n=14 (Tiam1+Bcr); n=19 (Bcr-GD).

N ≥ 3 independent experiments for each experiment shown. See also Figure S1.

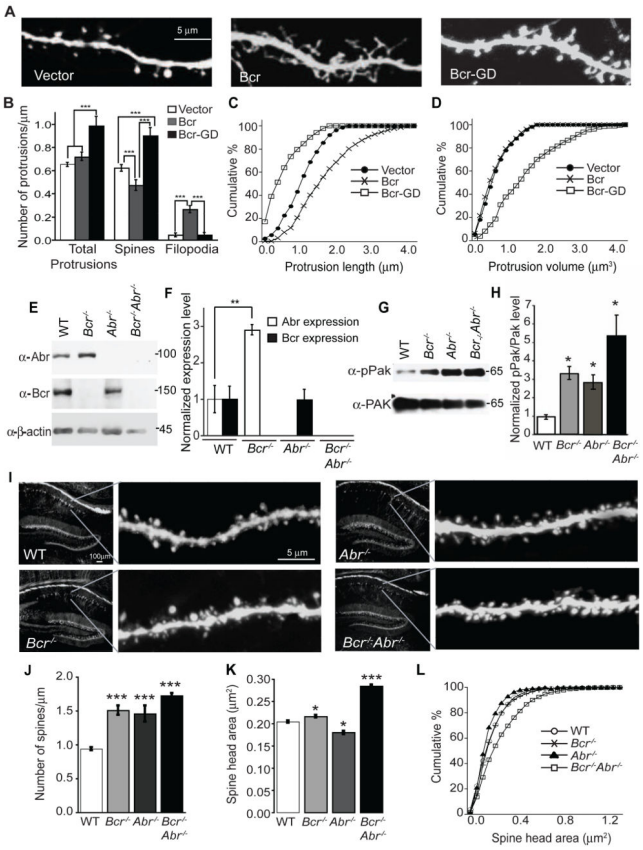

Figure 2. Bcr negatively regulates spine development by inhibiting Rac1 activity

(A and B) Dissociated rat hippocampal neurons (6–7 DIV) were transfected with eGFP and empty vector, Myc-Bcr, or Myc-Bcr-GD and imaged at 21 DIV. (A) Representative images. (B) Quantification of the density of total protrusions, spines and filopodia on neurons expressing vector (n=58), Bcr (n=32), or Bcr-GD (n=20).

(C and D) Cumulative percentage of protrusion length (C) and protrusion volume (D) of neurons expressing vector, Bcr, or Bcr-GD.

(E and F) Hippocampal lysates from P30 WT, *Bcr*$^{-/-}$, *Abr*$^{-/-}$, and *Bcr*$^{-/-}$*Abr*$^{-/-}$ mice were immunoblotted to determine the levels of Abr, Bcr and β-actin (loading control). (E) Representative blot. (F) Quantification of normalized Abr and Bcr expression level, represented as a ratio of Abr or Bcr over β-actin intensity. N=3.

(G and H) Hippocampal lysates from WT, *Bcr*$^{-/-}$, *Abr*$^{-/-}$, and *Bcr*$^{-/-}$*Abr*$^{-/-}$ mice were immunoblotted for pPak and Pak levels (G), and then pPak levels were quantified and represented as a ratio of pPak over Pak intensity (H). N=3.

(I) Confocal images of CA1 pyramidal neurons in hippocampal sections prepared from P28 YFP-expressing WT, *Bcr*$^{-/-}$, *Abr*$^{-/-}$, and *Bcr*$^{-/-}$*Abr*$^{-/-}$ mice.

(J and K) Quantification of spine density (J) and spine head area (K) of YFP-expressing WT, *Bcr*$^{-/-}$, *Abr*$^{-/-}$, and *Bcr*$^{-/-}$*Abr*$^{-/-}$ CA1 pyramidal neurons.

(L) Cumulative percentage of spine head area in YFP-expressing WT, *Bcr*$^{-/-}$, *Abr*$^{-/-}$, and *Bcr*$^{-/-}$*Abr*$^{-/-}$ neurons. For 2J-L, n=75 neurons for each genotype.

N ≥ 3 independent experiments for each experiment shown. Error bars indicate ± SEM; *p < 0.05, **p < 0.01, ***p < 0.001. See also Figures S2 and S3.

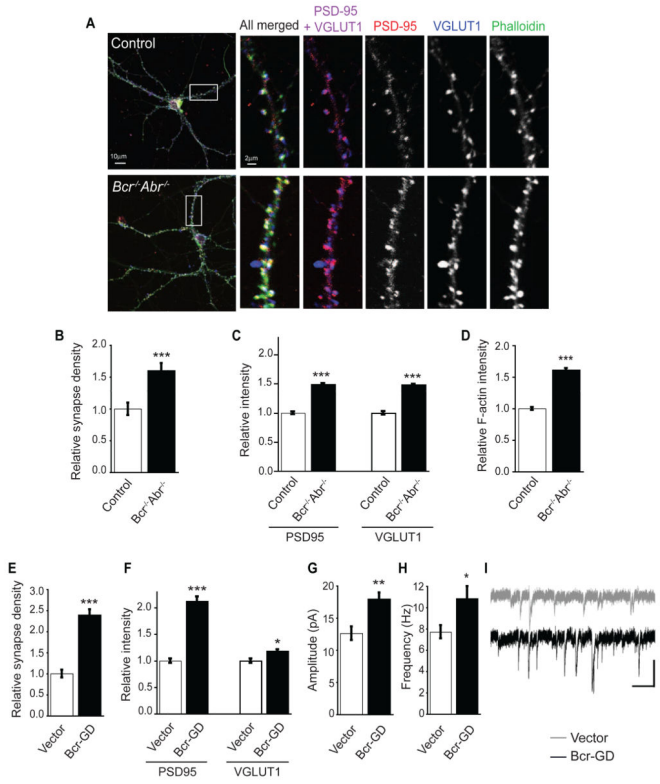

Figure 3. Bcr restricts excitatory synapse development

(A) 21 DIV dissociated hippocampal neurons from control ($Bcr^{+/-}Abr^{+/-}$) and $Bcr^{-/-}Abr^{-/-}$ mice were stained with antibodies against PSD-95 and VGLUT1 and with phalloidin.

(B) Quantification of synapse density. The number of colocalized PSD-95 and VGLUT1 puncta was counted and divided by dendritic area (μm^2) to determine synapse density and represented as relative synapse density. (n=31 neurons for control, n=39 for $Bcr^{-/-}Abr^{-/-}$).

(C) Quantification of relative intensity of PSD95 and VGLUT1 staining on control neurons (n=352 spines for PSD95, n=495 for VGLUT1) and $Bcr^{-/-}Abr^{-/-}$ neurons (n=335 for PSD95, n=480 for VGLUT1).

(D) Quantification of relative F-actin staining intensity on control (n=710 spines) and $Bcr^{-/-}Abr^{-/-}$ (n=317) neurons based on phalloidin staining.

(E, F) 21 DIV rat hippocampal neurons expressing eGFP with vector or Myc-Bcr-GD were immunostained with antibodies against PSD-95 and VGLUT1. (E) Relative synapse density was determined by counting the colocalized PSD-95 and VGLUT1 puncta per area of dendrite. (n=25 neurons per condition). (F) Quantification of relative intensity of PSD95 and VGLUT1 staining on neurons expressing vector (n=86 spines for PSD95, n=78 for VGLUT1) or Bcr-GD (n=138 for PSD95, n=128 for VGLUT1).

(G–I) Quantification of mEPSC amplitude (G) and frequency (H), and representative traces (I) from dissociated hippocampal neurons expressing vector (n=10 neurons) or Bcr-GD (n=10). Scale bar represents 200 ms and 20 pA.

N ≥ 3 independent experiments for each experiment shown. Error bars indicate ± SEM; *p < 0.05, **p<0.01, ***p < 0.001 for all graphs. See also Figure S3.

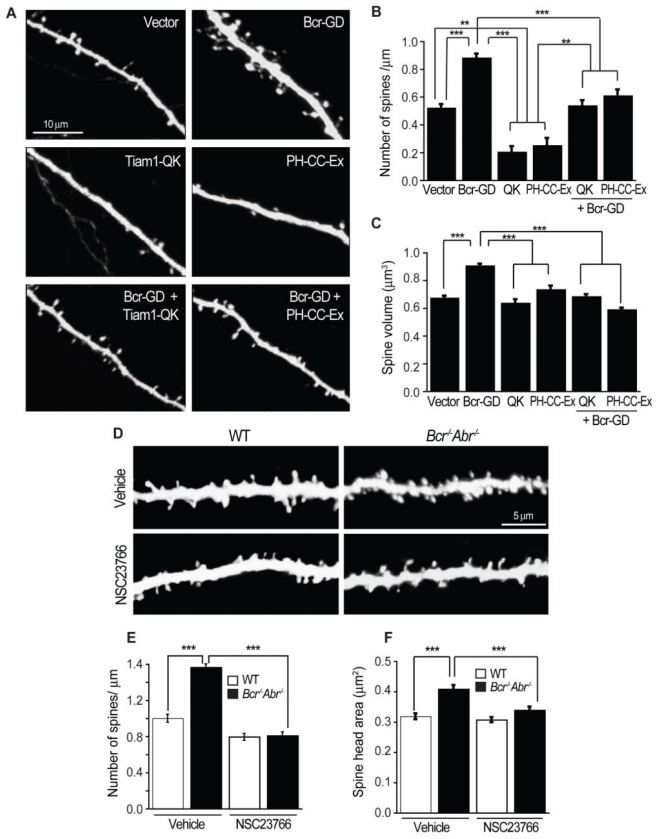

Figure 4. Bcr cooperates with Tiam1 to regulate Rac1-dependent spine development

(A) Dissociated rat hippocampal neurons expressing eGFP in combination with vector, Bcr-GD, Tiam1-QK, Tiam1-PH-CC-Ex, Bcr-GD + Tiam1-QK, or Bcr-GD + Tiam1-PH-CC-Ex were imaged at 21 DIV.

(B, C) Quantification of the density (B) and volume (C) of spines on neurons expressing vector (n=36 neurons), Bcr-GD (n=38), Tiam1-QK (n=18), Tiam1-PH-CC-Ex (n=12), Bcr-GD and Tiam1-QK (n=23), or Bcr-GD and Tiam1-PH-CC-Ex (n=23).

(D–F) Hippocampal slice cultures (17 DIV) prepared from YFP-expressing WT or $Bcr^{-/-}Abr^{-/-}$ mice were treated with the Tiam1 inhibitor NSC23766 (50 μM) or vehicle for 1 hr. YFP-positive CA1 pyramidal neurons were then imaged (D) and analyzed for total spine density (E) or the spine head area (F). n=75 neurons per condition.

All experiments were performed ≥ 3 independent times. Error bars represent ± SEM; **p<0.01, ***p<0.001 for all graphs. See also Figure S4.

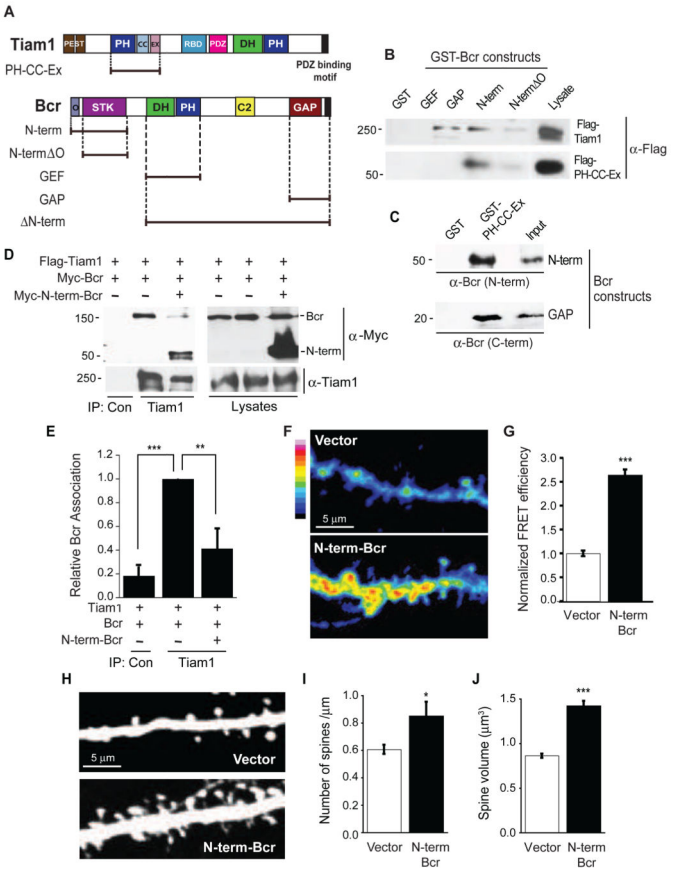

Figure 5. The Tiam1-Bcr interaction is essential for the regulation of Rac1 activity and spine development

(A) Domain structures of full-length and truncation mutants of Tiam1 and Bcr. **PEST**: PEST sequence; **PH**: pleckstrin homology domain; **CC-Ex**: coiled-coil and extended region; **RBD**: Ras-binding domain; PDZ: **PSD**-95/DlgA/ZO-1 domain; **DH**: Dbl homology domain; **O**: oligomerization domain; **STK**: serine/threonine kinase domain; **C2**: calcium-dependent lipid binding domain; **GAP**: GTPase-activating protein domain

(B) Lysates from COS7 cells expressing Flag-tagged Tiam1 or the Tiam1 PH-CC-Ex domain were incubated with the following bacterially-expressed GST-fused Bcr truncation mutants (GEF, GAP, N-term, and N-termΔO) or GST alone immobilized on beads. Precipitated proteins were analyzed by immunoblotting with anti-Flag antibodies.

(C) GST and the GST-tagged Tiam1 PH-CC-Ex domain immobilized on GSH beads were incubated with bacterially-expressed Bcr N-term or GAP domains (purified and cleaved from GST). Bound proteins were analyzed by immunoblotting with antibodies against Bcr's N- or C-terminus. The recombinant Bcr domains were also immunoblotted directly (input).

(D, E) Lysates from 293T cells expressing Flag-Tiam1 and Myc-Bcr in the presence or absence of Myc-N-term-Bcr were immunoprecipitated with an anti-Tiam1 antibody and immunoblotted with anti-Myc or anti-Tiam1 antibodies. (D) Representative western blot. (E) Quantification of the relative amount of Bcr coimmunoprecipitating with Tiam1. N=4 independent experiments.

(F, G) Rat hippocampal neurons expressing RaichuEV-Rac1 with vector (n=38) or Myc-N-term-Bcr (n=48) were imaged live at 17 DIV. Representative images are shown in the intensity-modulated display mode (F), and represented as relative mean FRET efficiency (G).

(H–J) Rat hippocampal neurons (6 DIV) were transfected with eGFP in combination with empty vector (n=22) or Myc-N-term-Bcr (n=14) and imaged at 21 DIV. (H) Representative images. (I, J) Quantification of the effects of N-term-Bcr overexpression on spine density (I) and spine volume (J).

All experiments were performed ≥ 3 independent times. Error bars represent ± SEM; *p<0.05, **p<0.01, ***p<0.001 for all graphs. See also Figure S5.

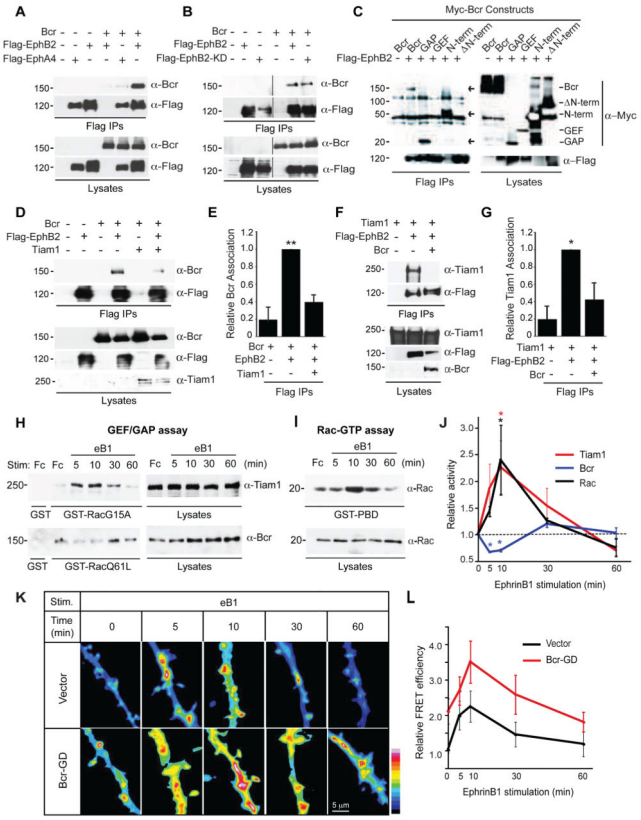

Figure 6. EphB receptors bind to Bcr and regulate the Tiam1-Bcr complex

(A) 293T cell lysates expressing Myc-Bcr alone or with Flag-tagged EphB2 or EphA4 were immunoprecipitated (IP) with anti-Flag antibodies, and then immunoblotted with anti-Bcr or anti-Flag antibodies. Lysates were also immunoblotted directly to confirm protein expression.

(B) 293T cell lysates expressing Myc-Bcr alone or with Flag-tagged EphB2 or EphB2-K.D. (kinase-dead) were immunoprecipitated with anti-Flag antibodies and immunoblotted with anti-Bcr or anti-Flag antibodies. The black line indicates removal of a nonessential lane between lanes 3 and 4.

(C) Flag-EphB2 was expressed in 293T cells alone or with Myc-tagged full-length Bcr or the following Bcr truncation mutants: GAP, GEF, N-term, or ΔN-term. EphB2 was immunoprecipitated with anti-Flag antibodies, and Bcr constructs were detected with anti-Myc antibodies. Despite causing reduced EphB2 expression, N-term Bcr interacted robustly with EphB2. Full-length Bcr and GAP also bound EphB2 (indicated by arrows).

(D, E) Lysates from 293T cells expressing Flag-EphB2 and Bcr in the presence or absence of Tiam1 were immunoprecipitated with anti-Flag antibodies, and then immunoblotted with anti-Bcr and anti-Flag antibodies to assess EphB2-Bcr binding. (D) Representative blot. Lysates were run on two different gels, one immunoblotted for Bcr and Flag the other immunoblotted for Tiam1. (E) Quantification of the relative amount of Bcr coimmunoprecipitating with Flag-EphB2. N=3 independent experiments.

(F, G) Lysates from 293T cells expressing Flag-EphB2 and Tiam1 in the presence or absence of Bcr were immunoprecipitated with anti-Flag antibodies, and then immunoblotted

with anti-Tiam1 antibodies to assess EphB2-Tiam1 binding. (F) Representative western blot. (G) Quantification of the relative amount of Tiam1 coimmunoprecipitated with Flag-EphB2. N=4 independent experiments.

(H–J) 21 DIV rat hippocampal neurons were stimulated with pre-clustered Fc or ephrinB1-Fc (eB1) for the indicated time points. (H) Lysates from these neurons were subjected to pull-down assays with GST (control), GST-Rac1-G15A (GEF assay) or GST-Rac1-Q61A (GAP assay), and then immunoblotted with anti-Tiam1 or anti-Bcr antibodies. (I) Lysates were subjected to pull-down assays with GST-PBD (Rac-GTP assay) and blotted with anti-Rac antibodies.

(J) Kinetics of Tiam1, Bcr and Rac1 activation in ephrinB1-stimulated rat hippocampal neurons. The levels of active Tiam1, Bcr and Rac were quantified from 3 independent experiments, and are represented as a ratio of Rac1-G15A-bound Tiam1, Rac1-Q61L-bound Bcr or Rac-GTP over total Tiam1, Bcr or Rac intensity, respectively.

(K, L) Rat hippocampal neurons expressing RaichuEV-Rac1 and empty vector (n=12–28) or Myc-Bcr-GD (n=12–20) were stimulated with pre-clustered eB1 for the indicated time points and then imaged live at 17 DIV. Representative images are shown in the intensity-modulated display mode (K) and represented as relative mean FRET efficiency (L).

For all experiments shown, $N \geq 3$ independent repeats. See also Figure S6.

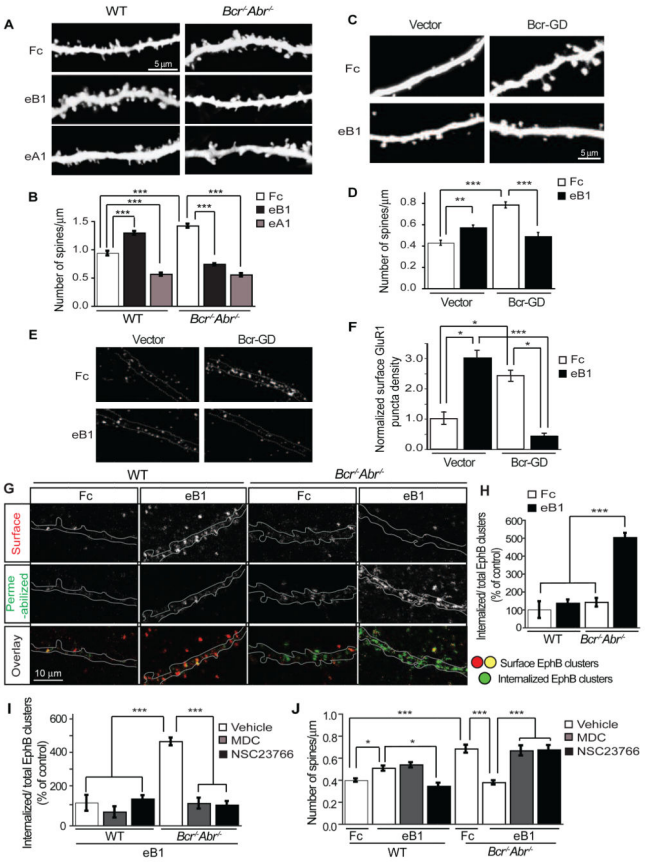

Figure 7. Bcr restricts Rac-dependent EphB internalization, preventing the conversion of ephrinB-induced spine growth into spine retraction

(A, B) Hippocampal slice cultures (17 DIV) from YFP-expressing WT or *Bcr*$^{-/-}$*Abr*$^{-/-}$ mice were stimulated with pre-clustered Fc, ephrinB1-Fc (eB1) or ephrinA1-Fc (eA1) for 1 hr. Following fixation, YFP-positive CA1 pyramidal neurons were imaged (A) and analyzed for spine density (B). n=75 neurons per condition.

(C) Representative images of 21 DIV rat hippocampal neurons expressing eGFP and vector or Myc-Bcr-GD that were stimulated with pre-clustered Fc or eB1 for 30 min.

(D) Quantification of the spine density on Fc- or eB1-stimulated neurons expressing vector (n=44 neurons for Fc and n=45 for eB1) or Myc-Bcr-GD (n=38 for Fc and n=30 for eB1).

(E, F) Surface GluR1 staining of Fc- or eB1-stimulated 21 DIV rat hippocampal neurons expressing vector or Myc-Bcr-GD. (E) Representative images. (F) Quantification of normalized surface GluR1 puncta density.

(G) Representative images of 21 DIV hippocampal neurons from WT and *Bcr*$^{-/-}$*Abr*$^{-/-}$ mice that were stimulated with Fc or eB1 for 30 min, and then live-cell stained for surface EphB-eB1 clusters. After surface labeling, neurons were fixed, permeabilized, and stained for the remaining EphB-eB1 clusters. Internalized clusters were identified as EphB clusters present in staining with permeabilization but absent in surface staining. In the overlay panel, surface EphB clusters are shown in red and yellow and internalized EphB clusters are in green.

(H) Quantification of Fc or eB1-induced EphB internalization in WT and *Bcr*$^{-/-}$*Abr*$^{-/-}$ neurons. EphB internalization was calculated as the ratio of internalized EphB clusters over total EphB clusters and represented as a percentage of EphB internalization in WT neurons. (I, J) Quantification of the effects of MDC or NSC23766 treatment on ephrinB-induced EphB internalization (I) or ephrinB-induced changes in spine density (J). 21 DIV hippocampal neurons (n=20–25) from WT and *Bcr*$^{-/-}$*Abr*$^{-/-}$ mice were pretreated with vehicle (DMSO), MDC or NSC23766, and then stimulated with pre-clustered Fc or eB1 for 30 min. Neurons were subjected to surface and permeabilized EphB-eB1 staining for EphB internalization analysis (I) or phalloidin staining for spine analysis (J).
All experiments were performed ≥ 3 independent times. Error bars represent ± SEM; *$p < 0.05$, **$p<0.01$, ***$p < 0.001$. See also Figures S4 and S7.